Dynamically assisted nuclear fusion in the strong-field regime

Martin Louis Lindsey [1,2] John Jasper Bekx [3] Karl-Georg Schlesinger,[3] and Siegfried Heinz Glenzer [2]
[1]*Institute for Computational & Mathematical Engineering, Stanford University, 475 Via Ortega, Stanford, California 94305, USA*
[2]*SLAC National Accelerator Laboratory, 2575 Sand Hill Road, Menlo Park, California 94025, USA*
[3]*Marvel Fusion, Theresienhöhe 12, 80339 Munich, Germany*

(Received 13 December 2022; revised 20 December 2023; accepted 12 March 2024; published 2 April 2024)

We consider quantum tunneling between fusing nuclei in the presence of a harmonically time-varying field. The tunneling rate is calculated using Floquet/Volkov (FV) and Kramers-Henneberger (KH) approaches, which are both compared to a first-principles numerical solution of the Crank-Nicolson (CN) type. Numerical validation of the FV approach justifies its use in analytical estimates of laser-enhanced reaction rates, while the KH approach does not reproduce the predictions of the others. For a deuterium-tritium plasma at a temperature of 1 keV, it is found that significant enhancement of fusion reactivity requires field strengths on the order of 10^{15}–10^{16} V/m and photon energies below 1 keV, which is within reach of next-generation x-ray free electron lasers (XFELs).

DOI: 10.1103/PhysRevC.109.044605

I. INTRODUCTION

Can extreme electromagnetic fields enhance the rate of fusion reactions in a realistic plasma? Access to a new regime of laser parameters [1–5] has directed attention toward the theoretical description of a number of processes affected or effected by the presence of such extreme fields. Examples include α- and proton-decay of atomic nuclei [6–8], electronic screening [9], and pair production, other QED processes in plasmas [10,11], and also nuclear excitations [12–16]. Of great significance among these types of laser-assisted processes is that of nuclear fusion [17–26], in large part due to the ever-growing need for an abundant source of clean energy. Fusion is the nuclear reaction central to the evolution and power output of every star in the universe [27]. First conceptualized just a decade after the famous mass-energy equivalence characterizing its exothermicity, this process eventually gained a theoretical description in the 1930s [28,29]. Over the subsequent nine decades, the scientific community has made gradual progress toward the production of a burning plasma [30–36]. The possible ability to enhance the reactivity in a plasma using ultraintense lasers could have major implications for the technological development of fusion power. Various approaches to modeling the effects of an ultraintense laser on fusion processes have been explored in recent works. Those employed can be largely categorized as semiclassical approaches: the Kramers-Henneberger (KH) approximation, and the Floquet-Volkoff (FV) method. Predictions are often restricted to particular cases, being made at isolated points [17,18] or sets of points [19–24] in the parameter range of interest. Our first work [25] made a systematic laser-parameter scan, which largely discredited the applicability of semiclassical methods for laser-enhancement predictions to nuclear fusion. In our second work [26] we showed that the remaining two methods display contradictory trends and in some cases, differ substantially.

Thus, to help resolve this ambiguity between analytical models, in this work we provide a robust estimate for the regime of field strengths and frequencies associated with the onset of substantial laser-enhanced fusion using a first-principles numerical solution of the Crank-Nicolson (CN) type. We show that the FV description leads to estimates that are in excellent agreement with those of the CN calculation over 10 orders of magnitude of variation. This analytical expression comes from the simplified picture in which pairs of fusing particles exchange an integer number of photons, each having energy $\hbar\omega$, with the laser field. On the other hand, the well-known KH description, in terms of a time-averaged, rapidly oscillating Coulomb barrier, leads to vastly different predictions. We conclude from this discrepancy that such a time-averaging procedure is unjustified. More details surrounding each employed method are deferred to the Appendixes. After having verified the FV method, we use it to estimate the laser-induced fusion enhancement to the overall reactivity in a thermalized plasma.

As an example case in the calculations to follow, we consider the deuterium-tritium (DT) reaction $^2\mathrm{H} + {}^3\mathrm{H} \rightarrow {}^4\mathrm{He} + n$, along with a range of laser parameters consistent with state-of-the-art x-ray free electron laser (XFEL) capabilities. This range is taken to include photon energies on the order of keV and electric field strengths on the order of 10^{15} V/m (laser intensities on the order of 10^{23} W/cm^2). The calculations throughout this work rely on the dipole approximation, meaning that the external field is always treated as spatially uniform. Note that this further implies the field has no magnetic component. It applies in this case, since both the laser wavelength and spot size are always much larger than the size of the two-particle system on which the fusion process is modeled. Under this approximation, the one-dimensional (1D) formulation of the original problem can be extended in a straightforward way to account for the external field [7].

II. GAMOW MODEL AND BEYOND

In the Gamow model of nuclear reactions, two particles with respective masses m_1 and m_2, charge numbers Z_1 and Z_2, and initial velocities $\mathbf{v}_1$ and $\mathbf{v}_2$ are considered in their center-of-momentum frame [27,37–39]. This model describes the process by which they fuse in three independent steps: (i) collision, (ii) tunneling, and (iii) nuclear interaction. Each step respectively contributes a term to the formula for the cross section σ of a fusion reaction:

$$\sigma(\mathcal{E}) = \underbrace{\frac{1}{\mathcal{E}}}_{\text{(i)}} \times \underbrace{\mathcal{T}(\mathcal{E})}_{\text{(ii)}} \times \underbrace{\mathcal{S}(\mathcal{E})}_{\text{(iii)}}, \tag{1}$$

having dimensions of area (SI units m^2). This physical quantity loosely corresponds—but is not equivalent—to the likelihood that a reaction occurs at a given center-of-mass energy $\mathcal{E} = \mu u^2/2$. Here, $\mu^{-1} = m_1^{-1} + m_2^{-1}$ defines the reduced mass μ of the particles, and $u = |\mathbf{v}_1 - \mathbf{v}_2|$ is their relative speed. The quantity $\mathcal{T}$ is the transparency factor, and $\mathcal{S}$ is the astrophysical S factor, which is often fitted by a polynomial [40,41]. Applying a strong external field is theorized to affect the tunneling probability in step (ii) by modifying the Coulomb potential, akin to tunnel ionization of atoms [42] or dissociation of molecules [43] in optical laser fields. While the field strengths of interest are extreme in the sense of modern laser capabilities, they are assumed to have a negligible effect on step (iii) directly, due to the nuclear potential having an energy scale that is many orders of magnitude larger [27,38,39]. Note that the geometric factor from step (i) is proportional to the square of de Broglie wavelength $\lambda\!\!\!^{-} = \hbar/\sqrt{2\mu\mathcal{E}}$. We emphasize that although the topic of laser-driven tunneling already enjoys an established place among scientific literature spanning several decades, it was not directly considered in the context of nuclear fusion until quite recently [17].

The transparency factor describes the probability that the particles tunnel through their mutual Coulomb repulsion to within reach of the attractive, short-range, strong nuclear force. This probability is calculated using the solution $\Psi(r,t)$ to the time-dependent Schrödinger equation (TDSE) describing their relative motion, where $r > 0$ is the interparticle separation. It has the form $i\hbar\frac{\partial\Psi}{\partial t} = (\frac{\mathbf{p}^2}{2\mu} + V)\Psi$, where $\mathbf{p}$ is the momentum and V is the potential. When applying the Wentzel-Kramers-Brillouin (WKB) approximation to express Ψ in the presence of a Coulomb potential $V_\mathrm{C}(r) = \kappa/r$ with $\kappa = e^2 Z_1 Z_2/4\pi\varepsilon_0$ and no external field, one obtains the eponymous Gamow factor,

$$\mathcal{T}(\mathcal{E}) = \exp^{-\mathcal{G}/\sqrt{\mathcal{E}}}, \tag{2}$$

where $\mathcal{G} = \pi\kappa\sqrt{2\mu}/\hbar$ is the Gamow constant [19,27]. Above, ε_0 is the vacuum permittivity and e is the elementary charge. Note that Eq. (2) is obtained by regarding the nuclear binding potential as a contact force, describing the formation of a pointlike compound nucleus in step (iii) by assuming that the particles must tunnel all the way to $r = 0$. Additionally, only the 1D radial solution is considered, meaning $\mathbf{p} \to -i\hbar\,\partial/\partial r\,\hat{\mathbf{r}}$, and contributions from TDSE solutions with nonzero angular momentum are neglected [27,38,39].

When extending the Gamow model to incorporate a dynamic external field $V_\mathrm{ext}(r,t)$, the transparency calculation still requires that the TDSE be solved, but now we must let $V(r,t) = V_\mathrm{C}(r) + V_\mathrm{ext}(r,t)$. The added time dependence makes the WKB approximation unsuitable [25], and the widely used imaginary time method [6,44,45] diverges in the frequency range of interest [25]. As a consequence, the semiclassical approximation must be abandoned altogether; however, the parameter range of interest still conveniently admits a nonrelativistic description of tunneling motion taking place within a classical electromagnetic field. The resulting TDSE presents an opportunity for the analytical FV and KH approaches to be compared, and benchmarked, against the numerical CN approach. In KH and CN, the nuclear binding region is modeled as having radius $R \approx 1.44(A_1^{1/3} + A_2^{1/3})$ in femtometers [18,27,38,39] rather than being pointlike, where A_1 and A_2 are the respective mass numbers of the fusing particles. Therefore, we apply as in [25] the multiplicative factor $\exp\{2\mathcal{G}[\sin^{-1}\sqrt{\rho} + \sqrt{\rho(1-\rho)}\,]/\pi\sqrt{\mathcal{E}}\}$ to Eq. (2), where $\rho = R\mathcal{E}/\kappa$, in order to account for this finite radius. Doing so also establishes a consistent value of the field-free transparency across all methods, allowing their predictions of the laser-modification effect to be reliably compared.

We consider a linearly polarized laser field, introducing the additional parameters A, θ, and ω to the tunneling problem. They respectively correspond to the vector potential magnitude, polarization angle (with respect to the interparticle motion), and angular frequency of the applied harmonic field. Applying the principle of minimal coupling, $\mathbf{p} \to \mathbf{p} + q\mathbf{A}\cos(\omega t)$, in the length gauge, and expanding the kinetic term leads to the external field

$$V_\mathrm{ext}(r,t) = U_\mathrm{q}\cos(\omega t) + 2U_\mathrm{p}\cos^2(\omega t) \tag{3}$$

to the Hamiltonian in the TDSE, where $U_\mathrm{q} = qAu\cos\theta$ and $U_\mathrm{p} = q^2A^2/4\mu$ are respectively quiver and pondermotive terms associated with the laser-driven oscillation. Here, $q/\mu = e(Z_1/m_1 - Z_2/m_2)$ defines the effective charge q of the particles in the 1D description. In the presence of a laser, the tunneling probability therefore depends on the multiparameter $\boldsymbol{\Xi} = (\mathcal{E}, A, \theta, \omega)$, and the dynamically modified transparency is accordingly denoted by $\mathcal{T}(\boldsymbol{\Xi})$. We assume, as in the original Keldysh [46] calculation of laser-induced tunneling ionization rates, that the external field comes in adiabatically at $t \to -\infty$. This allows the additional phase degree of freedom to be discarded from the argument of the sinusoidal functions in Eq. (3).

An expansion of Ψ can be sought in terms of a countably infinite "ladder" of basis states, each corresponding to the absorption or emission of an integer number of photons—this is the Floquet ansatz [47–49] mentioned by Queisser and Schützhold [17] and Kohlfürst *et al.* [20]. The coefficients in this expansion are derived by initially describing Ψ as a Volkov state [50–52] and then calculating its Fourier representation, as done by Wang [19] and also by Liu *et al.* [21]. Utilizing this FV approach, the resulting value of the

transparency is a superposition of terms resembling Eq. (2):

$$\mathcal{T}_{\mathrm{FV}}(\boldsymbol{\Xi}) = \sum_{n=-\infty}^{\infty} \left| J_n\left(\frac{U_\mathrm{q}}{\hbar\omega}, \frac{U_\mathrm{p}}{2\hbar\omega}\right)\right|^2 \mathcal{T}(\mathcal{E}_n)\,, \tag{4}$$

where $\mathcal{E}_n = \mathcal{E} + U_\mathrm{p} + n\hbar\omega$ are referred to as sideband energies. Here, $J_n(x, y)$ denote generalized Bessel functions [19,21], which satisfy the normalization property $\sum_{n\in\mathbb{Z}} |J_n(x, y)|^2 = 1$ for all $(x, y) \in \mathbb{C}^2$ [53,54]. To be precise, this solution is identified with an incident Floquet state having quasienergy $\mathcal{E} + U_\mathrm{p}$ and a discrete spectrum of sideband energy shifts $\pm n\hbar\omega$ for $n \in \mathbb{Z}$ induced by the surrounding laser field. It is simultaneously identified with a Volkov state describing an incident plane wave at energy $\mathcal{E}$ which is modulated by the unitary phase factor $\varphi(t) = \exp[-\frac{i}{\hbar}\int^t dt'\, V_{\mathrm{ext}}(t')]$ due to the presence of the surrounding laser field. This factor is sometimes referred to as the Volkov phase [51].

The complex conjugate of the Volkov phase, $\varphi^\dagger$, is also known as the KH transformation [18,20,21,24]. It gives rise to another strategy for solving the laser-modified TDSE: the tunneling problem is considered within an accelerating frame of reference in which the forces due to the external field vanish. In this case, the transformation is equivalent to performing the substitution $\mathbf{r} \mapsto \mathbf{r} - \mathbf{r}_\mathrm{q}$ on the three-dimensional (3D) spatial variable, where $\mathbf{r}_\mathrm{q}(\boldsymbol{\Xi}) = q\mathbf{A}(t)/\mu\omega$ is the laser-driven displacement characterizing the quiver motion of the KH frame. The tunneling potential appearing in the transformed Hamiltonian now oscillates, leading to the KH potential $V_{\mathrm{KH}}(r, t) = \kappa/|\mathbf{r} - \mathbf{r}_\mathrm{q}(t)|$, where the explicit dependence on A, θ, and ω has been suppressed. Assuming the oscillation period $\tau = 2\pi/\omega$ is very small compared to all other timescales, a static "effective potential," $V_{\mathrm{eff}}(r) = \frac{1}{\tau}\int_0^\tau dt\, V_{\mathrm{KH}}(r, t)$, can be obtained by taking the corresponding time average. This effective potential can then be substituted into the WKB formula [18,21–24] to provide an alternative estimate of the laser-modified transparency:

$$\mathcal{T}_{\mathrm{KH}}(\boldsymbol{\Xi}) = \exp\left\{-\frac{2\sqrt{2\mu}}{\hbar}\mathrm{Im}\left[\int_{r\in\mathcal{R}} dr\,\sqrt{V_{\mathrm{eff}}(r) - \mathcal{E}}\right]\right\}, \tag{5}$$

where $\mathcal{R} = \{r > R_{\mathrm{KH}} \,|\, V_{\mathrm{eff}}(r) > \mathcal{E}\}$ is the classically forbidden region. As assumed by Lv *et al.* [18,22,23], the shape swept out by the short-range spherical nuclear binding potential is taken to provide the interior classical turning point at R_{KH}. Further details regarding this inner binding region and the 1D form of V_{eff} are included in Appendix B. All relevant derivations are provided in extensive detail in Ref. [55].

Whether or not a time-averaged potential will provide a sufficiently accurate approximation to model laser-driven nuclear fusion holds great similarity to the use of the Keldysh parameter γ_K in optical ionization processes [46,56,57]. Just as how γ_K signifies the nonadiabaticity of the laser-driven tunneling of an electron, i.e., the extent to which it cannot be described in terms of a static potential, we may express a similar parameter γ_G, to the same end, defined as

$$\gamma_G = \omega\sqrt{2\mu\mathcal{E}}/(qE), \tag{6}$$

where the electric field strength $E = A\omega$. For relatively low-frequency oscillations ($\gamma_G < 1$), a quasistatic treatment proves to be sufficient and is referred to as the adiabatic or strong-field regime, whereas high-frequency oscillations ($\gamma_G > 1$) allow for the use of time-averaged quantities and is referred to as the multiphoton regime. Up to a redefinition of parameters μ and q, each driven tunneling problem (atomic ionization, α decay, nuclear fusion) is equivalent from a mathematical standpoint. However, the physical scales (distances and time intervals set by incident energy $\mathcal{E}$) associated with each problem differ vastly, affecting which assumptions can be made, and subsequently, which models are applicable.

III. NUMERICAL VALIDATION

The CN method [58] is well suited to the 1D TDSE of interest [7,59]. Our setup involves a Gaussian wave packet initialized inside of the nuclear binding region where the external field is set to zero, in accordance with the transparency factor describing solely the tunneling step of the fusion process. The wave packet proceeds to scatter against the laser-modified Coulomb barrier from the inside, encountering the external field no sooner than it enters the classically forbidden region. While technically this is a simulation of the tunneling step in a (fictional) nuclear-decay process, the symmetry between it and the opposite-direction tunneling process is a standard [27,38] justification for such an approach to the fusion transparency. The main advantage of this setup is that its initial conditions are constructed from exact solutions to the potential within the starting region, which is not the case when a wave packet is placed initially on the outside of the barrier. We also verify that when supplied with no external field, the CN results are consistent with Eq. (2). Further details of the numerical algorithm can be found in Appendix C. Though the use of the CN method for Gaussian-wave-packet propagation and tunneling does not provide a complete description of the complicated process of nuclear fusion, it does provide a first-principles calculation for the tunneling transparency against which the prior analytical methods can be benchmarked, and is novel in the field of laser-enhanced fusion.

IV. CONTRADICTING THEORETICAL PREDICTIONS

We compare the values of $\mathcal{T}(\boldsymbol{\Xi})$ resulting from each method for center-of-mass energies between 0.1 and 10 keV within a range of $\boldsymbol{\Xi}$ space approaching that characterizing state-of-the-art laser parameters. Figures 1 and 2 show the laser-modified transparency predicted by each method, with the former and latter respectively depicting electric field strengths of $E = 10^{15}$ V/m and $E = 10^{16}$ V/m. The upper subplots compare different external field frequencies, while the lower subplots compare different polarization angles. It is clear that the FV and CN approaches are in good agreement. Both predict that tunneling at higher center-of-mass energies is unaffected outside of extremely high field strengths, and that the presence of the laser leads to nonzero transparencies even in the limit $\mathcal{E} \to 0$. Such low-$\mathcal{E}$ behavior leads, for example, to increases in over 10 orders of magnitude below a center-of-mass energy of 0.5 keV in Figs. 1 and 2. Above a center-of-mass energy of 2–3 keV in these figures, no enhancement effect can be seen. This trend is conceptually

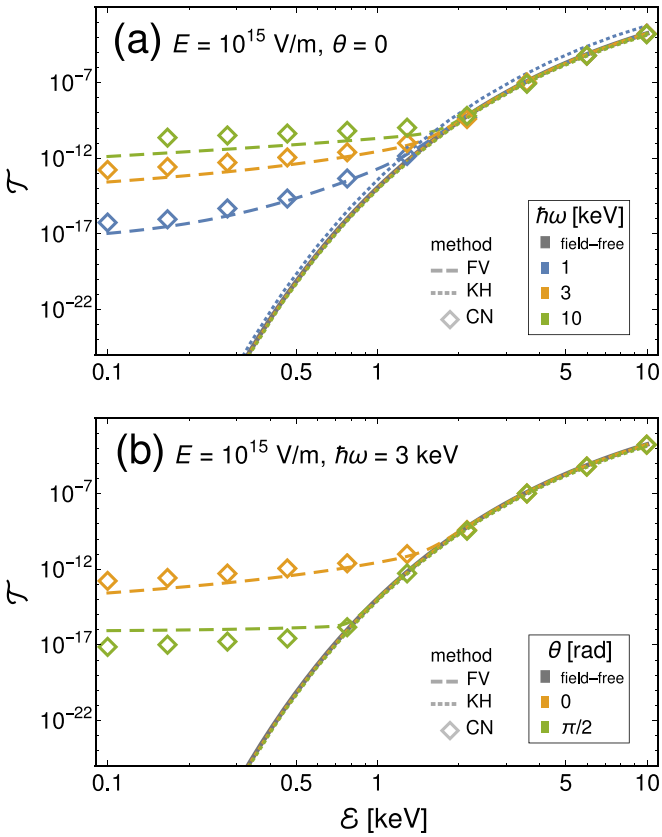

FIG. 1. Comparison of modified transparency estimates using FV (dashed curves), KH (dotted curves), and CN ($\diamond$s) for the DT fusion reaction as a function of center-of-mass energy. The field strength is fixed at $E = 10^{15}$ V/m; (a) the polarization angle is fixed at $\theta = 0$, while the photon energy is chosen to be 1 keV (blue), 3 keV (orange), and 10 keV (green); (b) the photon energy is fixed at $\hbar\omega = 3$ keV, while the polarization angle is chosen to be 0 (orange) and $\pi/2$ (green). The gray solid curve is the field-free transparency.

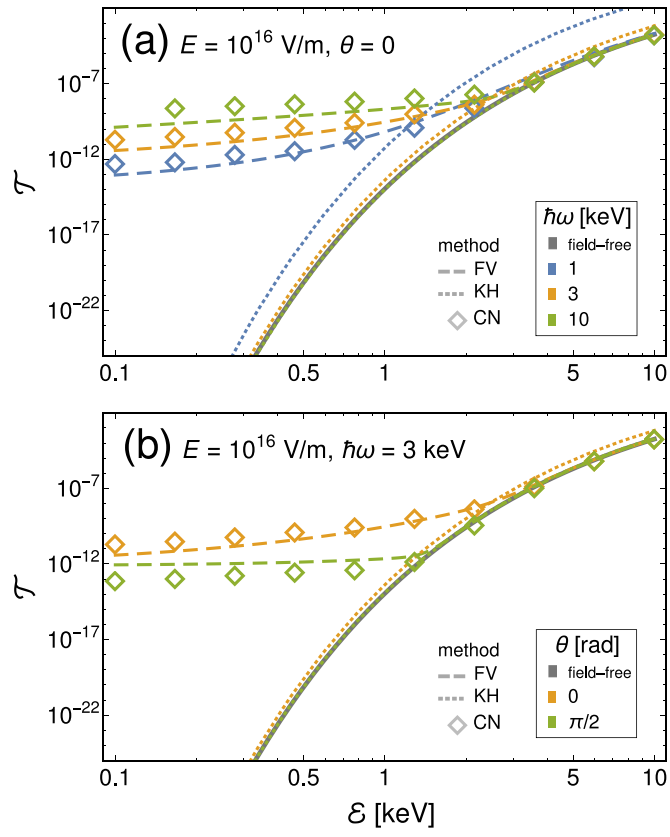

FIG. 2. Higher-field-strength version of Fig. 1, where now $E = 10^{16}$ V/m, with all other parameters unchanged.

consistent with a modest amount of energy gain during tunneling. Indeed, the behavior of the sideband energy $\mathcal{E}_n$ for large n as $\mathcal{E} \to 0$ in Eq. (4) suggests that a sufficiently intense laser field allows particles that were initially at rest with respect to one another to fuse by absorbing photon energy. The enhancement effect at low $\mathcal{E}$ increases significantly with field strength and also increases with frequency until exhibiting a saturation phenomenon as $\hbar\omega$ increases beyond 10 keV. A comparison between Figs. 1(a) and 2(a) further demonstrates that the transparency is more sensitive to increases in field strength at low $\hbar\omega$. Symmetry with respect to the θ parameter causes all transparency curves to lie between two extremes (at $\theta = 0$ and $\theta = \pi/2$), as shown in Figs. 1(b) and 2(b); they all closely approximate the orange ($\theta = 0$) transparency, except for a narrow range of angles very close to $\pi/2$. Notably, the CN results do not appear to reflect the subtle behavior of the $E = 10^{16}$ V/m, $\hbar\omega = 1$ keV, $\theta = 0$ dashed curve (blue) of Fig. 2(a), which actually overtakes its higher-frequency counterparts (orange and green) in the center-of-mass energy range $1 \leqslant \mathcal{E} \leqslant 5$ keV.

In contrast to the other methods, the KH approach leads to transparency estimates with major differences. It predicts an enhancement effect that is independent of center-of-mass energy. Moreover, it fails to reproduce the significant increase in transparency at low $\mathcal{E}$ predicted by FV and CN, predicting instead that the laser-modified transparency vanishes in the $\mathcal{E} \to 0$ limit like in the field-free case. It is also far less sensitive to changes in $\hbar\omega$. The only prediction that KH has in common with the other methods is that the enhancement effect is more sensitive to increases in E at lower $\hbar\omega$. This markedly different behavior may be interpreted in terms of the shape of $V_{\text{eff}}(r)$ as a result of time averaging: the peak of the Coulomb barrier is lowered slightly and is also brought a small distance out from the origin, which changes the tunneling problem drastically. The inconsistency between KH and the numerical result casts doubt on the viability of the simplified expression V_{eff} within the range of parameters considered here. Consequently, we identify the analytical FV expression in Eq. (4) as a suitable extension of the Gamow transparency factor in Eq. (2) to the dynamic-field case, due to its overall consistency with CN predictions within the parameter range of interest. This numerical validation of the FV formula enables an analytical calculation of the laser-enhanced reactivity for a kinetic distribution of many particles.

V. LASER-ENHANCED REACTIVITY

In a system of particles described by a distribution $f(\mathcal{E}, \theta)$ over center-of-mass energies and polarization angles, the overall number of fusion reactions per unit time is directly

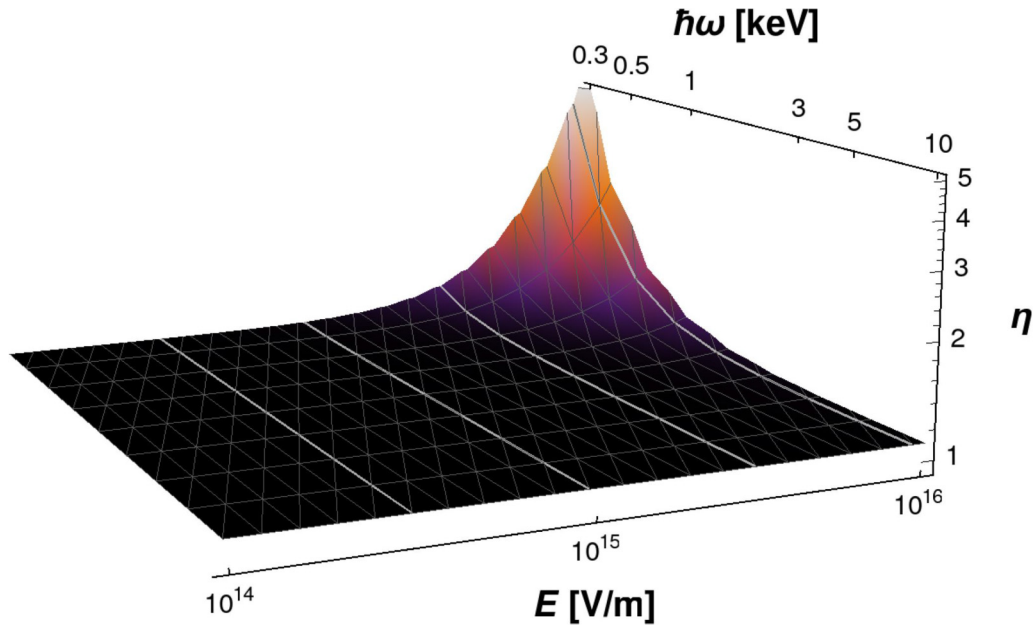

FIG. 3. Enhancement factor $\eta = \langle \sigma_{\rm FV}(\Xi)u\rangle/\langle\sigma(\mathcal{E})u\rangle$ associated with the strong-field fusion reactivity in a thermal DT plasma at temperature $k_{\rm B}T = 1$ keV, calculated for a range of photon energies and field strengths. Height is also characterized by color, with the transition from black to violet indicating the $\eta \geqslant 2$ threshold. The highlighted curves in gray mark the values $E = \{3\times10^{14}, 1\times10^{15}, 3\times10^{15}, 1\times10^{16}\}$ V/m for reference. At sufficiently high field strengths ($E \geqslant 5\times10^{16}$ V/m), enhancement factors of around a factor of two are calculated toward the lower range of photon energies ($\hbar\omega \approx 200$ eV) marking the beginning of the soft-x-ray band. All axes are log scale.

proportional to the reactivity

$$\langle \sigma u\rangle = \int d\mathcal{E} \int d\theta\, f(\mathcal{E},\theta)\sigma(\mathcal{E})\sqrt{\frac{2\mathcal{E}}{\mu}}, \tag{7}$$

which has dimensions of volume per unit time (SI units m^3/s). We take f to have the Maxwell-Boltzmann form, using the factorization $f(\mathcal{E},\theta) = f(\mathcal{E})f(\theta)$ assuming thermal equilibrium. The standard probability density $f(\mathcal{E}) = 2\sqrt{\mathcal{E}/\pi}\,(k_{\rm B}T)^{-3/2}\exp^{-\mathcal{E}/k_{\rm B}T}$ in terms of temperature T with $k_{\rm B}$ the Boltzmann constant is used for center-of-mass energies [27], and the probability density $f(\theta) = \frac{1}{2}\sin\theta$ corresponding to 3D isotropy is used for polarization angles $0 \leqslant \theta \leqslant \pi$. Assuming the frequency of the external field at XFEL photon energies is high enough, the incident wave Ψ is well described by a Volkov state long before arriving within tunneling range. The sideband expansion can thus be applied to all of $\sigma(\mathcal{E})$ rather than just $\mathcal{T}(\mathcal{E})$, now giving a superposition of terms resembling Eq. (1). We substitute this superposition into Eq. (7) to obtain an analytical estimate for the laser-enhanced fusion reactivity. It is worth noting that this substitution can be performed irrespective of the form of the velocity distribution f, meaning that it is also applicable to beam-beam/beam-target and nonthermal settings as well. Keep in mind also that A and ω are the only free parameters that remain after integrating over $\mathcal{E}$ and θ.

Figure 3 depicts a surface plot of the resulting enhancement factor with respect to the field-free reactivity, as a function of electric field strength and photon energy, for a DT plasma at a temperature of $k_{\rm B}T = 1$ keV. It is assumed this plasma has been prepared before the interaction with the XFEL pulse. We find no enhancement effect below an electric field strength of 10^{15} V/m at any of the frequencies considered, with an increase of a factor of ≈5 requiring field strengths closer to 10^{16} V/m at low photon energies. The laser-enhanced fusion reactivity decreases with increasing $\hbar\omega$, which is simply a consequence of the trend shown by the dashed curves in Fig. 2(a). At small $\hbar\omega$, the absorption and emission probabilities are high, so the $n > 1$ sidebands are sufficiently populated for a significant fraction of the incident wave to tunnel at a higher energy, as discussed by Wang [19]. Conversely, at large $\hbar\omega$ the sideband spectrum is sharply peaked at about $n = 0$, and thus tunneling effectively occurs at $\mathcal{E}$ regardless of the laser input. To significantly increase the occupancy of higher-order sidebands at large $\hbar\omega$ (i.e., greater than 3 keV), field strengths at or above 10^{17} V/m would be required. Note that the largest enhancements are found in the strong-field regime. The lower limit on the photon energies in Fig. 3 was imposed, as below this value we found the FV results start to deviate from the CN results beyond an order of magnitude at the largest of the electric field strengths considered. This can be understood by considering γ_G [Eq. (6)]. As $\hbar\omega$ is lowered, keeping all other parameters fixed, we traverse from the multiphoton regime ($\gamma_G > 1$) into the strong-field regime ($\gamma_G < 1$). In the intermediate region $\gamma_G \approx 1$, the temporal scale of harmonic oscillation of the laser field $\sim\cos(\omega t)$ becomes comparable to that of the tunneling. Thus, the phase ϕ of the laser field, omitted in Eq. (3), will lead to an effect on the transparency in this regime. Assuming $\phi = 0$ as we do imposes the largest contribution from the harmonic laser field to occur at the start of the tunneling. At a different phase $\phi \in (0, 2\pi)$, this value is diminished, thus explaining why the FV method overestimates the transparency when $\gamma_G \approx 1$. The lower limit on $\hbar\omega$ is of

course smaller for lower values of the electric field strength, since $\gamma_G \sim \omega/E$.

VI. CONCLUSIONS AND OUTLOOK

After accounting for all collision geometries present in an equilibrium distribution of particles, our calculations indicate that the thermal reactivity of a DT plasma at a temperature of 1 keV can be enhanced by up to a modest factor of $\approx$5 by the application of a laser, provided sufficiently extreme electric fields in the range 10^{15}–10^{16} V/m and photon energies in the range 0.3–1 keV are used. It is interesting to note that the threshold field strength predicted here is appreciably below the Schwinger limit of around 10^{18} V/m. We conclude that ultraintense, soft x-ray fields should be most effective at enhancing the thermal DT reactivity. These predictions of laser-modified reactivity are justified by first-principles numerical calculations, which we find to be consistent with the FV description of the fusion tunneling process and inconsistent with the time-averaged KH description.

The laser parameters associated with the greatest enhancement factors in Fig. 3 are just beyond the range of peak intensities demonstrated by current state-of-the-art XFELs but may be feasible in the not-too-distant future. The predictions shown in this work suggest that ultraintense XFELs have the potential to access parameter regimes consistent with observable enhancements to laser-driven plasma fusion. Additional effects of, e.g., higher dimensions, electronic screening, and laser pulse shaping on the tunneling problem were neglected to arrive at an analytical expression for the laser-enhanced fusion cross section consistent with first-principles numerical calculations. This enhancement process is demonstrated to have a sound theoretical basis and is worthy of investigation in further detail. In order for it to be a practical avenue towards fusion power development, the enhancement would have to exceed the various loss mechanisms (bremsstrahlung, heat conduction, volume expansion) in a given fusing plasma, dependent on the manner in which the plasma is created, the target geometry, plasma properties, its environment, among many other factors. This sort of technological consideration is beyond the scope of this work.

ACKNOWLEDGMENTS

We would like to acknowledge support from the DOE Office of Science, Fusion Energy Science, under Grant No. FWP 100182. This work was also partially supported by the National Science Foundation under Grant No. 2308860. This work is supported in part by the U.S. Department of Energy (DOE), Office of Science, Fusion Energy Sciences, under Award No. DE-SC 0024882:IFE-STAR.

APPENDIX A: REQUISITE ASSUMPTIONS AND APPLICABILITY

As mentioned in the main text, all results presented make use of the dipole approximation. This assumption places an upper bound on the values of $\hbar\omega$ (found to be $\approx$12 keV) below which we would expect our predictions to apply, due to the dispersion relation $\omega = c/\lambda$. To this end, there are two length scales we must consider: (I) the typical separation r that the nuclei "start from" when they undergo mutual scattering, and (II) the thickness of the potential barrier. Seeking a rough characterization of experimentally realistic settings, we find that for a distribution of particles at thermal equilibrium with number density $\approx 10^{23}\,\mathrm{cm}^{-3}$ and temperature $\approx$1 keV, the laser wavelength λ is much greater than both (I) and (II) within the parameter range of interest. Analogously to our spatial scales, there are two timescales we must also consider: (I) the collision time, i.e., the time taken outside of the barrier to reach the classical turning point, and (II) the traversal time, i.e., the "time spent under" the potential barrier during the tunneling motion. This latter timescale tends to be much shorter than the former; note that it is, however, purely imaginary-valued and stems from a semiclassical interpretation despite its practical utility [46]. We summarize the conditions for applicability with respect to these timescales for our methods below:

(1) For the time-averaging step in the KH approach, the oscillation period of the laser is shorter than (II).
(2) For the FV approach [and thus the laser-enhanced reactivity calculation which substitutes Eq. (4) into Eq. (7) in the main text], the time required to populate the Floquet ladder is shorter than (I). Note that due to the nuclear-decay configuration of the CN simulations, their agreement with FV suggests that the timescale to populate the most significant sidebands is actually much shorter than (I), below even (II) at the parameters considered. The FV and KH methods also require lower bounds to be established for ω, since both of their respective formulas break down in the static-field limit $\omega \to 0$ for $A \neq 0$. This lower bound on $\hbar\omega$ is found to be around 300 eV for center-of-mass energies on the keV scale and field strengths between 10^{14} and 10^{16} V/m. We emphasize here that in contrast, the CN approach possesses no such lower bound, since no additional assumptions are made about the incident wave, potential barrier, or external field.

APPENDIX B: THEORETICAL METHODS

1. Floquet/Volkov approach

The FV approach bears resemblance to both the Volkov-state analyses of Wang [19] and Liu *et al.* [21], as well as the Floquet picture discussed by Queisser and Schützhold [17]. We start from the TDSE, which now contains the external potential from Eq. (3) in the main text, reading

$$i\hbar\frac{\partial}{\partial t}\Psi = \Bigg[-\frac{\hbar^2}{2\mu}\frac{\partial^2}{\partial r^2} + V_C(r) + \underbrace{U_\mathrm{q}\cos(\omega t) + 2U_\mathrm{p}\cos^2(\omega t)}_{V_\mathrm{ext}} \Bigg]\Psi. \tag{B1}$$

Its solution $\Psi(r,t)$ can be written in terms of $\psi(r)$, the solution to the field-free Schrödinger equation at center-of-mass energy $\mathcal{E}$, which reads $[-\frac{\hbar^2}{2\mu}\frac{\partial^2}{\partial r^2} + V_C(r)]\psi = \mathcal{E}\psi$. This latter

TDSE corresponds to the original time-independent tunneling problem solved by the Gamow factor in Eq. (2) from the main text. The Volkov phase $\phi(t)$ effectively modulates the harmonic term $e^{-i\mathcal{E}t/\hbar}$ associated with the energy eigenvalue of the field-free TDSE, which leads to

$$\Psi(r,t) = \psi(r)e^{-i\mathcal{E}t/\hbar} \underbrace{\exp\left[-\frac{i}{\hbar}\int^t dt'\, V_{\text{ext}}(t')\right]}_{\varphi(t')}, \tag{B2}$$

for the solution to Eq. (B1). Assuming a simple harmonic external field, the Volkov phase evaluates to

$$\begin{aligned}\varphi(t) &= \exp\left[i\frac{U_\text{q}}{\hbar\omega}\sin(\omega t) + i\frac{U_\text{p}}{2\hbar\omega}\sin(2\omega t)\right]e^{-iU_\text{p}t/\hbar} \\ &= \sum_{n\in\mathbb{Z}} J_n\left(\frac{U_\text{q}}{\hbar\omega}, \frac{U_\text{p}}{2\hbar\omega}\right)e^{-in\omega t}e^{-iU_\text{p}t/\hbar},\end{aligned} \tag{B3}$$

where $J_n(x,y)$ are the generalized Bessel functions [53,54]. They appear as a result of taking a Fourier transform, or equivalently, applying the Jacobi-Anger identity $e^{iz\sin(\omega t)} = \sum_{n\in\mathbb{Z}} J_n(z)e^{in\omega t}$ twice—once to each term in the square brackets in the first line above. Combining Eqs. (B2) and (B3), the solution to (B1) becomes

$$\begin{aligned}\Psi(r,t) &= \psi(r)e^{-i\mathcal{E}t/\hbar}\left[\sum_{n\in\mathbb{Z}} J_n\left(\frac{U_\text{q}}{\hbar\omega}, \frac{U_\text{p}}{2\hbar\omega}\right)e^{-i(U_\text{p}+n\hbar\omega)t/\hbar}\right] \\ &= \sum_{n\in\mathbb{Z}} J_n\left(\frac{U_\text{q}}{\hbar\omega}, \frac{U_\text{p}}{2\hbar\omega}\right)\underbrace{\psi(r)e^{-i(\mathcal{E}+U_\text{p}+n\hbar\omega)t/\hbar}}_{\psi_{\mathcal{E}+U_\text{p}+n\hbar\omega}},\end{aligned} \tag{B4}$$

up to a phase factor that is of no importance to our analysis. Equation (B4) possesses the form of a Floquet expansion at quasienergy $\mathcal{E}+U_\text{p}$. Since the field-free solutions ψ (and also their Bessel function prefactors) are orthonormal, Eq. (B4) is readily substituted into the expression $\mathcal{T} = |\psi(\infty)|^2/|\psi(R)|^2$ that gave rise to the field-free Gamow factor. Only the diagonal terms in the product-sum survive when taking $|\Psi|^2$, and the aforementioned phase factors are eliminated as well, justifying their earlier omission. This summation formula describes the laser-modified solution as a discrete, infinite "Floquet ladder" of field-free states with spacing $\hbar\omega$ between energy levels. The discrete probability mass function on this ladder is $P_n = |J_n(\frac{U_\text{q}}{\hbar\omega}, \frac{U_\text{p}}{2\hbar\omega})|^2$ for $n\in\mathbb{Z}$, which is canonically interpreted as representing absorption ($n>0$) and emission ($n<0$) of integer numbers of photons. In practice, the Floquet expansion is truncated below at

$$\nu(\mathcal{E},E,\omega) = \min\{n\in\mathbb{Z}\,|\,\mathcal{E}+U_\text{p}+n\hbar\omega \geqslant 0\},$$

due to the restriction that sidebands with negative kinetic energy do not contribute to the transparency are disallowed in the expansion. Note that the FV method does not allow for a consideration of static fields, as the results diverge for $\omega\to 0$. By its inherent design, i.e., the construction of the Floquet ladder of sidebands, the method is best suited for the multiphoton regime. This leads to a lower limit on ω, which depends on the value of the electric field strength, that was discussed in the main text. Beyond this limit, static-field extensions to the Gamow model ought to be employed instead (Refs. [25,26]).

2. Kramers-Henneberger approach

The KH analysis follows the discussion in Lv *et al.* [18,22,23] and Liu *et al.* [21]. We must go back and consider the full 3D two-body problem before reformulating it in 1D. Applying the KH phase factor to arrive at $\Psi_\text{KH}(\mathbf{r},t) = \phi(t)\Psi(\mathbf{r},t)\phi^\dagger(t)$ is equivalent to the coordinate transformation $\mathbf{r}\to\mathbf{r}-\mathbf{r}_\text{q}(t) = \mathbf{r}_\text{KH}(t)$, where the displacement vector

$$\mathbf{r}_\text{q}(t) = \frac{q}{\mu\omega}\mathbf{A}\cos(\omega t) \tag{B5}$$

describes the laser-driven "quiver motion" of the oscillating reference frame. This oscillation has amplitude $r_\text{q} = |\mathbf{r}_\text{q}|$ and is aligned in the same direction as the external field—note that the angle parameter θ from Ξ has not yet been introduced, as the problem has yet to be cast into 1D.

The transformed TDSE now reads $i\hbar\frac{\partial}{\partial t}\Psi_\text{KH} = [-\frac{\hbar^2}{2\mu}\nabla^2 + V_C(\mathbf{r}_\text{KH})]\Psi_\text{KH}$, which closely resembles the time-independent field-free problem. To obtain the 1D reduction, the Legendre polynomials $P_\ell(z)$ defined for $\ell\in\mathbb{N}$ and $z\in[-1,1]$ may be employed [18,22,23]. These special functions have the property

$$\frac{1}{|\mathbf{r}-\mathbf{r}'|} = \begin{cases}\frac{1}{r}\sum_{\ell=0}^\infty P_\ell(\cos\theta)\left(\frac{r'}{r}\right)^\ell & \text{if } r>r' \\ \frac{1}{r'}\sum_{\ell=0}^\infty P_\ell(\cos\theta)\left(\frac{r}{r'}\right)^\ell & \text{if } r<r',\end{cases} \tag{B6}$$

where $r' = |\mathbf{r}'|$, and θ is defined by $\mathbf{r}\cdot\mathbf{r}' = rr'\cos\theta$. When applying Eq. (B6) to the transformed potential $V_\text{KH}(\mathbf{r},t) = V_C(\mathbf{r}_\text{KH}(t))$, we simply multiply it through by κ and perform the replacement $\mathbf{r}'\to\mathbf{r}_\text{q}(t)$, as done by Lv *et al.* [18] to arrive at a 1D formula $V_\text{KH}(r,t)$ for the KH potential. Next, to eliminate the time dependence, an average is taken over one oscillation period $\tau = 2\pi/\omega$ of the external field, leading to an effective potential of the form $V_\text{eff}(r) = \frac{1}{\tau}\int_0^\tau dt V_\text{KH}(r,t)$. Note that although the initial consideration of the KH potential keeps the full time dependence as a series expansion around the zero-mode average [60], in practice only this static averaged component is considered [18,21–23] most suited as a quasistatic approximation for high values of $\hbar\omega$.

The time-averaging procedure also implies that the nuclear binding region of the effective potential is extended to take on a "capsulelike" shape [18,22,23]. More precisely, it is the subset $\mathcal{B}_\text{KH}\subset\mathbb{R}^3$ swept out by a sphere of radius R whose center is displaced from the origin by $\mathbf{r}_\text{q}(t)$ over one oscillation period. This elongated nuclear binding region can be written

$$\mathcal{B}_\text{KH} = \bigcup_{t\in[0,\tau]}\{\mathbf{r}\,|\,\mathbf{r}_\text{KH}(t) < R\}. \tag{B7}$$

Equation (B7) leads to the following 1D analytical expression for the KH nuclear radius $R\to R_\text{KH}$ as a function of θ, which is simply a parametrization of the boundary $\partial\mathcal{B}_\text{KH}$ in polar

coordinates:

$$R_{\mathrm{KH}}(\theta) = \begin{cases} r_{\mathrm{q}}\cos\theta + \frac{1}{2}\sqrt{4R^2 - 2r_{\mathrm{q}}^2(1+\cos 2\theta)}, & \text{if } \theta \in \Theta_1 \\ \frac{R}{\sin\theta}, & \text{if } \theta \in \Theta_2 \\ \frac{1}{2}\sqrt{4R^2 - 2r_{\mathrm{q}}^2(1+\cos 2\theta)} - r_{\mathrm{q}}\cos\theta, & \text{if } \theta \in \Theta_3 \end{cases}, \tag{B8}$$

where $\Theta_1 = [0, \arctan\frac{R}{r_{\mathrm{q}}})$, $\Theta_2 = [\arctan\frac{R}{r_{\mathrm{q}}}, \pi - \arctan\frac{R}{r_{\mathrm{q}}})$, and $\Theta_3 = [\pi - \arctan\frac{R}{r_{\mathrm{q}}}, \pi]$. No explicit form of the potential is required here for $r < R_{\mathrm{KH}}$, since that is where the WKB transparency integral stops. With the value of $R_(\theta)$ specified, we proceed with the 1D reduction. The time-averaged potential has an analytical solution outside of the nuclear binding region, which Lv *et al.* [18] also describe:

$$V_{\mathrm{eff}}(r) = \frac{\kappa}{r_{\mathrm{q}}}\sum_{\ell\in 2\mathbb{N}} P_\ell(\cos\theta)\begin{cases} \frac{1}{\pi}\big[\sum_{j=1}^{\ell/2}\gamma_\ell\zeta\sqrt{1-\varrho^2}(\varrho^{\ell-2j} - \varrho^{2j-\ell-2}) + \frac{2\gamma_\ell}{\sqrt{\pi}}\big(\varrho^{-\ell-1}\xi - \varrho^\ell\log\tan\frac{\xi}{2}\big)\big], & \text{if } \varrho < 1 \\ \frac{\gamma_\ell}{\sqrt{\pi}}\varrho^{-\ell-1}, & \text{if } \varrho > 1, \end{cases} \tag{B9}$$

for all $r > R_{\mathrm{KH}}$ (or equivalently, $r \in \mathbb{R}^3\ \mathcal{B}_{\mathrm{KH}}$), where the dimensionless quantities

$$\gamma_\ell = \frac{\Gamma\left(\frac{\ell+1}{2}\right)}{\Gamma\left(\frac{\ell+2}{2}\right)}, \quad \zeta = \frac{\Gamma(i)}{\Gamma\left(i+\frac{1}{2}\right)},$$
$$\varrho = \frac{r}{r_{\mathrm{q}}}, \quad \xi = \arcsin\varrho,$$

are introduced here to streamline the formula slightly. Note that the full dependence on the multiparameter Ξ in Eqs. (B7), (B8), and (B9) has been suppressed. The KH transparency factor is finally obtained by evaluating $\mathcal{T}_{\mathrm{KH}}$ using V_{eff} defined in Eq. (B9) above, as well as the interval

$$\mathcal{R} = \left[R_{\mathrm{KH}}, V_{\mathrm{KH}}^{-1}(\mathcal{E})\right] \subset \mathbb{R}_+ \tag{B10}$$

for the classically forbidden region. The inner turning point R_{KH} is given by Eq. (B8), and the outer turning point is given by $V_{\mathrm{KH}}^{-1}(\mathcal{E})$, which solves the equation $V_{\mathrm{eff}}(r) = \mathcal{E}$.

As a final remark, the formula for $R_{\mathrm{KH}}(\theta)$ provided in Eq. (B8) differs from that in [26], which amounts to $R_{\mathrm{KH}} = \min\{\frac{R}{\sin\theta}, R + r_{\mathrm{q}}\}$. While the above definition characterizes a subset of $\mathbb{R}^3$ of similar size and dimension to $\mathcal{B}_{\mathrm{KH}}$, it is actually a close approximation, with the advantage of having a simpler expression. Notably, the above definition and Eq. (B8) coincide exactly at $\theta = \pi/2$ and also at $\theta = 0$, which are consistent with all data shown in Figs. 1 and 2 in the main text, as well as all results shown in Ref. [26].

APPENDIX C: NUMERICAL METHOD

1. Crank-Nicolson approach

A discrete representation of the wave function in space is required for numerical computation: $\Psi(r,t) \to \{\Psi(j\Delta x, t)\}_{j\in[M]} = \Psi_t \in \mathbb{C}^M$ at each point in time t, where M is the number of grid points, spaced apart by a distance Δx, in the spatial domain. The expression $[M] = \{1, 2, \ldots, M\}$ is set-container notation. For sufficiently small Δt, Ψ_t can be numerically time evolved as $\Psi_{t+\Delta t} \approx \exp(-\frac{i}{\hbar}H\Delta t)\Psi_t$ by using an approximation to the time-evolution operator. The Hamiltonian $H \in \mathbb{C}^{M\times M}$ takes on a matrix representation, which means that the time-evolution operator is, in turn, a matrix exponential. The original CN scheme makes use of the first diagonal Padé approximant,

$$\exp\left(-\frac{i}{\hbar}H\Delta t\right) \approx \left(\mathbb{1} - \frac{i\Delta t}{2\hbar}H\right)^{-1}\left(\mathbb{1} + \frac{i\Delta t}{2\hbar}H\right), \tag{C1}$$

to this matrix exponential, where $\mathbb{1}$ is the $M \times M$ identity matrix. Including the time derivative of the Hamiltonian [7,59] yields the linear system

$$\left(\mathbb{1} - i\frac{\Delta t}{2\hbar}H - i\frac{\Delta t^2}{4\hbar^2}\dot{H}\right)\Psi_{t+\Delta t} = \left(\mathbb{1} + i\frac{\Delta t}{2\hbar}H + i\frac{\Delta t^2}{4\hbar^2}\dot{H}\right)\Psi_t \tag{C2}$$

to solve at each time step, where the dot denotes the time derivative. When using the standard second-difference formula for the Laplacian in the kinetic energy operator, the Hamiltonian matrix appearing in Eq. (C2) has special tridiagonal structure, which is particularly convenient for numerical solution. This structure can be expressed as

$$\left[-\frac{\hbar^2}{2\mu}\frac{\partial^2}{\partial r^2} + V(r,t)\right]$$
$$\to H = \frac{\hbar^2}{2\mu\Delta x^2}\begin{pmatrix} \ddots & 1 & & \\ 1 & -2 & 1 & \\ & 1 & -2 & 1 \\ & & 1 & \ddots \end{pmatrix} + V,$$

where $V = \mathrm{diag}(V_t) \in \mathbb{R}^{M\times M}$ is a diagonal matrix containing the spatial discretization of the instantaneous potential as its entries: $V(r,t) \to \{V(j\Delta x, t)\}_{j\in[M]} = V_t \in \mathbb{R}^M$ at each point in time t. For a modest accuracy boost, we employ the further approximation $H(t + \frac{1}{2}\Delta t) \approx H(t) + \frac{\Delta t}{2}\dot{H}(t)$ of Mišicu and Rizea [7,8], exploiting the fact that an explicit formula for the time derivative of the Hamiltonian is known for all $t \in \mathbb{R}$. Since this Taylor expansion only introduces another diagonal term, its impact on computational performance is negligible. Letting N denote the total number of time steps, this algorithm has a scaling of $O(MN)$. Note that this scaling would be $O(M^3N)$ if naive matrix inversion were used rather than

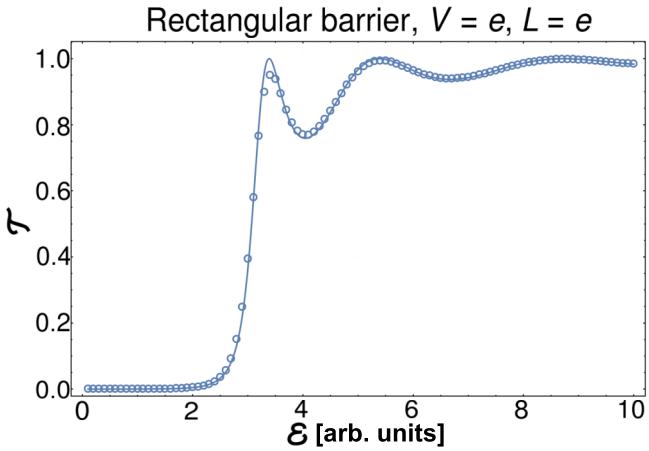

FIG. 4. Comparison between analytic and numerical results for a rectangular barrier of height and width $V = L = e$ in arbitrary units. The CN calculations successfully capture the sharp increase near $\mathcal{E} = e$ and the oscillatory behavior at higher energies. The first peak, which is sharpest, is slightly underestimated due to the Gaussian blur effect, as further elaborated on in the text.

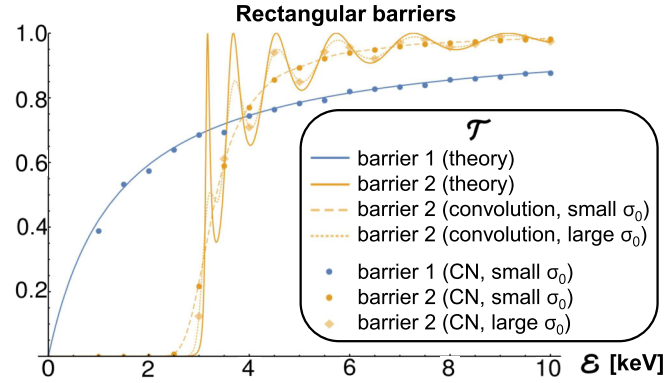

FIG. 5. Gaussian blur of the numerical transparency curve resulting from the spectral width of the incident wavepacket. Barrier 2 (orange) refers to a short, wide rectangular barrier like in Fig. 4, and barrier 1 (blue) is a tall, thin rectangular barrier that exhibits similar properties to the Coulomb barrier. The value of σ_0 in Eq. (C3) is lowered to demonstrate the extent of the blurring effect. Note that the 'nodes' in the above-barrier oscillation are least affected, while the peaks and troughs are most affected.

making efficient use of its tridiagonality. The initial condition is a Gaussian wave packet, having continuous representation

$$\Psi(r,0) = \frac{e^{-ikr}}{(\pi\sigma_0^2)^{1/4}} \exp\left[-\frac{(r-x_0)^2}{2\sigma_0^2}\right], \tag{C3}$$

with de Broglie wave number $k = \sqrt{2\mu\mathcal{E}}/\hbar$, and the Gaussian distribution $\mathcal{N}(x_0, \sigma_0^2)$ defining its probability density on the r axis. This $t = 0$ solution is discretized into a vector and supplied as the input to the first linear system in the iteration.

2. Rectangular barrier for benchmarking

It is well established [58,61,62] that the CN method exhibits oscillatory numerical artifacts. These oscillations can be viewed as a consequence of the discrete spatial grid only being able to represent certain wavelengths. Since the oscillations become significant when discontinuities appear in the initial or boundary conditions, a "big-box" setup is used in this work, wherein the spatial grid (i.e., the parameter M) is large enough that the amplitude of the wave packet goes to zero before reaching the boundary, mitigating these oscillations.

To benchmark the CN method, we use it to calculate the transparency through a rectangular barrier of height V and width L, which can be compared to its analytical expression:

$$\mathcal{T}(\mathcal{E}) = \left\{1 + \frac{V^2 \sinh^2\left[\frac{L}{\hbar}\sqrt{2\mu(V-\mathcal{E})}\right]}{4\mathcal{E}(V-\mathcal{E})}\right\}^{-1}. \tag{C4}$$

For numerical convenience, arbitrary units are used in which $\hbar = 1$ and energies and lengths are scaled accordingly. The values $V = e$ and $L = e$ are chosen along with an energy range of $0.1 \leqslant \mathcal{E} \leqslant 10$, in arbitrary units, in order to reproduce the characteristic above-barrier oscillation in the transparency curve. A comparison between the numerical and analytic transparency curves for the rectangular barrier is shown in Fig. 4. It demonstrates excellent agreement between the two methods, supporting the use of CN for other potential barriers.

The underestimation of the sharpest peak in Fig. 4 stems from an artifact known as Gaussian blurring. It is a subtlety that stems from the use of Gaussian wave packets to model the behavior of pure plane-wave states. As the value of the transparency is calculated in terms of pure plane waves, and a wave packet is an infinite (continuous) superposition of plane-wave states, it follows that the resulting value of $\mathcal{T}$ contains contributions from each component k of the wave packet. This can be recovered exactly as an expectation over the probability density in k space that defines the Gaussian envelope. In momentum space, the representation of a wave packet is given by $P_k \propto e^{-(k-k_0)^2/\varsigma^2}$, where $k_0 = \sqrt{2\mu\mathcal{E}}/\hbar$ is the peak of the k-space distribution, which corresponds to the incident energy $\mathcal{E}$ of the idealized plane wave in the Gamow model. The value of ς is the reciprocal of the spatial width σ_0 from Eq. (C3) for the x-space representation, which is related through its associated Fourier transform. The wave-packet transparency thus has the form

$$\mathcal{T}_{\text{wave packet}} \propto \int dk\, \mathcal{T}(k) e^{-(k-k_0)^2/\varsigma^2}, \tag{C5}$$

i.e., that of a convolution with a Gaussian kernel. Gaussian kernels blur the data with which they are convolved, which in this case produces a blurry transparency curve compared to the plane-wave estimate. More precisely, it brings every point on the curve closer to its local (i.e., binned) average. This is most apparent in the case of the oscillating rectangular barrier transparency discussed previously, as depicted in Fig. 5 below. Note that wave packets that are highly localized in x space have very broad distributions in k space. Consequently, convergence to the plane-wave estimate is achieved in the limit $\sigma_0 \to \infty$. Fortunately, the monotonicity

of the field-free (as well as modified) Gamow transparency curves makes them less sensitive to Gaussian blur, as the contributions from $k < k_0$ effectively "cancel out" those coming from $k > k_0$.

[1] A. V. Bashinov, A. A. Gonoskov, A. V. Kim, G. Mourou, and A. M. Sergeev, New horizons for extreme light physics with mega-science project XCELS, Eur. Phys. J. Spec. Top. **223**, 1105 (2014).

[2] A. S. Pirozhkov, Y. Fukuda, M. Nishiuchi, H. Kiriyama, A. Sagisaka, K. Ogura, M. Mori, M. Kishimoto, H. Sakaki, N. P. Dover *et al.*, Approaching the diffraction-limited, bandwidth-limited petawatt, Opt. Express **25**, 20486 (2017).

[3] S. Gales, K. A. Tanaka, D. L. Balabanski, F. Negoita, D. Stutman, O. Tesileanu, C. A. Ur, D. Ursescu, I. Andrei, S. Ataman *et al.*, The extreme light infrastructure—Nuclear physics (ELI-NP) facility: New horizons in physics with 10 PW ultra-intense lasers and 20 MeV brilliant gamma beams, Rep. Prog. Phys. **81**, 094301 (2018).

[4] C. N. Danson, C. Haefner, J. Bromage, T. Butcher, J.-C. F. Chanteloup, E. A. Chowdhury, A. Galvanauskas, L. A. Gizzi, J. Hein, D. I. Hillier *et al.*, Petawatt and exawatt class lasers worldwide, High Power Laser Sci. Eng. **7**, e54 (2019).

[5] M. Jirka, O. Klimo, and M. Matys, Relativistic plasma aperture for laser intensity enhancement, Phys. Rev. Res. **3**, 033175 (2021).

[6] A. Pálffy and S. V. Popruzhenko, Can extreme electromagnetic fields accelerate the α decay of nuclei? Phys. Rev. Lett. **124**, 212505 (2020).

[7] Ş. Mişicu and M. Rizea, α-decay in ultra-intense laser fields, J. Phys. G: Nucl. Part. Phys. **40**, 095101 (2013).

[8] Ş. Mişicu and M. Rizea, Laser-assisted proton radioactivity of spherical and deformed nuclei, J. Phys. G: Nucl. Part. Phys. **46**, 115106 (2019).

[9] D. Elsing, A. Pálffy, and Y. Wu, Quantum effects on plasma screening for thermonuclear reactions in laser-generated plasmas, Phys. Rev. Res. **4**, L022004 (2022).

[10] A. Di Piazza, C. Müller, K. Z. Hatsagortsyan, and C. H. Keitel, Extremely high-intensity laser interactions with fundamental quantum systems, Rev. Mod. Phys. **84**, 1177 (2012).

[11] N. Narozhny and A. Fedotov, Extreme light physics, Contemp. Phys. **56**, 249 (2015).

[12] A. Dadi and C. Müller, Laser-assisted nuclear photoeffect, Phys. Rev. C **85**, 064604 (2012).

[13] A. Pálffy and H. A. Weidenmüller, Laser-nucleus reactions: population of states far above Yrast and far from stability, Phys. Rev. Lett. **112**, 192502 (2014).

[14] A. Pálffy, O. Buss, A. Hoefer, and H. A. Weidenmüller, Laser-nucleus interactions: The quasi-adiabatic regime, Phys. Rev. C **92**, 044619 (2015).

[15] L. von der Wense, P. V. Bilous, B. Seiferle, S. Stellmer, J. Weitenberg, P. G. Thirolf, A. Pálffy, and G. Kazakov, The theory of direct laser excitation of nuclear transitions, Eur. Phys. J. A **56**, 176 (2020).

[16] S. Kobzak, H. A. Weidenmüller, and A. Pálffy, Laser-nucleus interactions in the sudden regime, Phys. Rev. C **103**, 044616 (2021).

[17] F. Queisser and R. Schützhold, Dynamically assisted nuclear fusion, Phys. Rev. C **100**, 041601(R) (2019).

[18] W. Lv, H. Duan, and J. Liu, Enhanced deuterium-tritium fusion cross sections in the presence of strong electromagnetic fields, Phys. Rev. C **100**, 064610 (2019).

[19] X. Wang, Substantially enhanced deuteron-triton fusion probabilities in intense low-frequency laser fields, Phys. Rev. C **102**, 011601(R) (2020).

[20] C. Kohlfürst, F. Queisser, and R. Schützhold, Dynamically assisted tunneling in the impulse regime, Phys. Rev. Res. **3**, 033153 (2021).

[21] S. Liu, H. Duan, D. Ye, and J. Liu, Deuterium-tritium fusion process in strong laser fields: Semiclassical simulation, Phys. Rev. C **104**, 044614 (2021).

[22] W. Lv, B. Wu, H. Duan, S. Liu, and J. Liu, Phase-dependent cross sections of deuteron-triton fusion in dichromatic intense fields with high-frequency limit, Eur. Phys. J. A **58**, 54 (2022).

[23] W. Lv, H. Duan, and J. Liu, Enhanced proton-boron nuclear fusion cross sections in intense high-frequency laser, Nucl. Phys. A **1025**, 122490 (2022).

[24] B. Wu, H. Duan, and J. Liu, Resonant tunneling of deuteron-triton fusion in strong high-frequency electromagnetic fields, Phys. Rev. C **105**, 064615 (2022).

[25] J. J. Bekx, M. L. Lindsey, S. H. Glenzer, and K.-G. Schlesinger, Applicability of semiclassical methods for modeling laser-enhanced fusion rates in a realistic setting, Phys. Rev. C **105**, 054001 (2022).

[26] J. J. Bekx, M. L. Lindsey, and K.-G. Schlesinger, Effect of nuclear charge on laser-induced fusion enhancement in advanced fusion fuels, Phys. Rev. C **106**, 034003 (2022).

[27] D. D. Clayton, *Principles of Stellar Evolution and Nucleosynthesis*, 2nd ed. (The University of Chicago Press, Chicago, IL, 1983).

[28] G. Gamow, The quantum theory of nuclear disintegration, Nature (London) **122**, 805 (1928).

[29] H. A. Bethe, Energy production in stars, Phys. Rev. **55**, 434 (1939).

[30] W. C. Elmore, E. M. Little, and W. E. Quinn, Neutrons of possible thermonuclear origin, Phys. Rev. Lett. **1**, 32 (1958).

[31] V. P. Smirnov, Tokamak foundation in USSR/Russia 1950–1990, Nucl. Fusion **50**, 014003 (2010).

[32] J. H. Nuckolls, Early steps toward inertial fusion energy (IFE) (1952 to 1962), United States: N. p., 1998.

[33] G. L. Kulcinski, M. E. Sawan, and I. N. Sviatoslavsky, Nuclear design and analysis of ITER: Progress report, November 15, 1987–November 14, 1988. United States: N. p., 1988. Web.

[34] P. Rodriguez-Fernandez, A. J. Creely, M. J. Greenwald, D. Brunner, S. B. Ballinger, C. P. Chrobak, D. T. Garnier, R. Granetz, Z. S. Hartwig, N. T. Howard *et al.*, Overview of the SPARC physics basis towards the exploration of burning-plasma regimes in high-field, compact tokamaks, Nucl. Fusion **62**, 042003 (2022).

[35] A. B. Zylstra, O. A. Hurricane, D. A. Callahan, A. L. Kritcher, J. E. Ralph, H. F. Robey, J. S. Ross, C. V. Young, K. L. Baker, D. T. Casey *et al.*, Burning plasma achieved in inertial fusion, Nature (London) **601**, 542 (2022).

[36] A. L. Kritcher, C. V. Young, H. F. Robey, C. R. Weber, A. B. Zylstra, O. A. Hurricane, D. A. Callahan, J. E. Ralph, J. S. Ross,

K. L. Baker *et al.*, Design of inertial fusion implosions reaching the burning plasma regime, Nat. Phys. **18**, 251 (2022).
[37] G. Gamow, Zur quantentheorie des atomkernes, Z. Phys. **51**, 204 (1928).
[38] J. M. Blatt and V. F. Weisskopf, *Theoretical Nuclear Physics*, 2nd ed. (Springer-Verlag, New York, 1979).
[39] S. Atzeni and J. Meyer-ter-Vehn, *The Physics of Inertial Fusion: Beam Plasma Interaction, Hydrodynamics, Hot Dense Matter* (Oxford University Press, Oxford, UK, 2004).
[40] H.-S. Bosch and G. M. Hale, Improved formulas for fusion cross-sections and thermal reactivities, Nucl. Fusion **32**, 611 (1992).
[41] H.-S. Bosch and G. M. Hale, Improved formulas for fusion cross-sections and thermal reactivities, Nucl. Fusion **33**, 1919 (1993).
[42] E. Mevel, P. Breger, R. Trainham, G. Petite, P. Agostini, A. Migus, J.-P. Chambaret, and A. Antonetti, Atoms in strong optical fields: Evolution from multiphoton to tunnel ionization, Phys. Rev. Lett. **70**, 406 (1993).
[43] R. N. Coffee, L. Fang, and G. N. Gibson, Light-induced potentials ignite dissociation of N_2^{+2}, Phys. Rev. A **73**, 043417 (2006).
[44] L. P. Kotova, A. M. Perelomov, and V. S. Popov, Quasiclassical approximation in ionization problems, Zh. Eksp. Teor. Fiz. **54**, 1151 (1968) [Sov. Phys. JETP **27**, 616 (1968)].
[45] S. V. Popruzhenko, V. D. Mur, V. S. Popov, and D. Bauer, Strong field ionization rate for arbitrary laser frequencies, Phys. Rev. Lett. **101**, 193003 (2008).
[46] L. V. Keldysh, Ionization in the field of a strong electromagnetic wave, Zh. Eksp. Teor. Fiz. **47**, 1945 (1965) [Sov. Phys. JETP **20**, 1307 (1965)].
[47] J. H. Shirley, Interaction of a quantum system with a strong oscillating field, Ph.D. thesis, California Institute of Technology, 1963.
[48] M. Grifoni and P. Hänggi, Driven quantum tunneling, Phys. Rep. **304**, 229 (1998).
[49] R. Merlin, Rabi oscillations, Floquet states, Fermi's golden rule, and all that: Insights from an exactly solvable two-level model, Am. J. Phys. **89**, 26 (2021).
[50] D. M. Wolkow, Über eine klasse von Lösungen der Diracschen Gleichung, Z. Phys. **94**, 250 (1935).
[51] D. Kidd, C. Covington, Y. Li, and K. Varga, Volkov basis for simulation of interaction of strong laser pulses and solids, Phys. Rev. B **97**, 024303 (2018).
[52] A. Di Piazza, Completeness and orthonormality of the Volkov states and the Volkov propagator in configuration space, Phys. Rev. D **97**, 056028 (2018).
[53] G. N. Watson, A *Treatise on the Theory of Bessel Functions*, 2nd ed. (Cambridge Mathematical Library, 1995).
[54] H. R. Reiss and V. P. Krainov, Generalized Bessel functions in tunnelling ionization, J. Phys. A: Math. Gen. **36**, 5575 (2003).
[55] M. L. Lindsey, Laser modification of nuclear fusion cross-sections, Ph.D. Thesis, Stanford University, 2023.
[56] V. S. Popov, Tunnel and multiphoton ionization of atoms and ions in a strong laser field (Keldysh theory), Phys.-Usp. **47**, 855 (2004).
[57] S. V. Popruzhenko, Keldysh theory of strong field ionization: History, applications, difficulties and perspectives, J. Phys. B: At. Mol. Opt. Phys. **47**, 204001 (2014).
[58] J. Crank and P. Nicolson, A practical method for numerical evaluation of solutions of partial differential equations of the heat-conduction type, Adv. Comput. Math. **6**, 207 (1996).
[59] Ş. Mişicu and M. Rizea, Emission of electromagnetic radiation in α-decay, J. Phys. G: Nucl. Part. Phys. **27**, 993 (2001).
[60] W. C. Henneberger, Perturbation method for atoms in intense light beams, Phys. Rev. Lett. **21**, 838 (1968).
[61] D. Britz, O. Østerby, and J. Strutwolf, Damping of Crank–Nicolson error oscillations, Comput. Biol. Chem. **27**, 253 (2003).
[62] O. Østerby, Five ways of reducing the Crank–Nicolson oscillations, BIT Numer. Math. **43**, 811 (2003).